RSC Advances

ROYAL SOCIETY OF CHEMISTRY

www.rsc.org/advances

Production of biochars from Ca impregnated ramie biomass (*Boehmeria nivea* (L.) Gaud.) and their phosphate removal potential

Shao-bo Liu [a, b], Xiao-fei Tan[c, d]*, Yun-guo Liu[c, d]*, Yan-ling Gu [c, d], Guang-ming Zeng[c, d], Xin-jiang Hu[c, d], Hui Wang[c, d], Lu Zhou [c, d], Lu-hua Jiang[c, d], Bin-bin Zhao[c, d]

[a] School of Metallurgy and Environment, Central South University, Changsha 410083, PR China

[b] School of Architecture and Art, Central South University, Changsha 410082, PR China

[c] College of Environmental Science and Engineering, Hunan University, Changsha 410082, P.R. China

[d] Key Laboratory of Environmental Biology and Pollution Control (Hunan University), Ministry of Education, Changsha 410082, P.R. China

* Corresponding author at: College of Environmental Science and Engineering, Hunan University, Changsha 410082, PR China. Tel.: + 86 731 88649208; Fax: + 86 731 88822829; E-mail address: hnuliuyunguo@gmail.com (Y.G. Liu); tanxf@hnu.edu.cn (X.F. Tan).

Abstract

This work explored the efficiency and mechanisms of phosphate (P) removal by Ca-impregnated biochar prepared from $CaCl_2$-pretreated ramie stem (Ca-RSB) and ramie bark (Ca-RBB). The properties of Ca-modified biochar were analyzed using elemental analyzer, scanning electron microscopy (SEM), BET specific surface analyzer, energy-dispersive X-ray analysis (EDS), Fourier transform infrared (FTIR) and zeta potential meter. The results of characterizations suggested that the resulted Ca-RSB had much higher H/C ratio, total pore volume, BET surface area and functional groups compared with pristine biochar (RSB). In addition, a higher yield of Ca-RSB (50.8%) than

RSB (28.0%) was also observed. Comparison experiments suggested that Ca-RSB showed higher adsorption capacity than Ca-RBB and the adsorption amount of Ca-RSB were more than two-folds than that of RSB. Adsorption experimental data fitted well with pseudo-second order kinetics and Langmuir isotherm. The intra-particle diffusion and Boyd's film-diffusion models revealed that the rate-controlled step was controlled by film-diffusion initially and then followed by intra-particle diffusion. Electrostatic attraction served as the main force to adsorb phosphate at lower pH, and the precipitation and surface deposition took over at higher pH. The results of this study indicated that Ca-RSB is a potential effective and low-cost adsorbent for phosphate removal from wastewater.

Keywords: Biochar; Calcium; Phosphate; Ramie (*Boehmeria nivea* (L.) Gaud.); Adsorption

1. Introduction

Phosphorus (P) is an essential element for the growth of all organisms and plants. However, excessive discharge of P into water can pose a significant threat to ecosystem, which is the most common cause of eutrophication in aqueous system including coastal marine, freshwater lakes, reservoirs and streams [1, 2]. Therefore, it is obligatory to remove phosphate from wastewater before discharging into water bodies [3]. There are a wide range of technologies, which can be applied to remove phosphorus from wastewater, such as chemical precipitation, biological phosphorus removal (application of microorganisms and constructed wetlands), adsorption and crystallisation technologies [3, 4].

Biochar is a carbon-rich material produced from different feedstocks including crop residues, wood biomass, animal litters, and solid wastes via various thermochemical processes (e.g., slow pyrolysis, fast pyrolysis, hydrothermal carbonization, flash carbonization and gasification) in an oxygen-limited condition [5, 6], which can be applied into soil with the benefits of both soil amendment and carbon sequestration [7, 8]. Considering its wide availability of feedstock and favorable physical/chemical characteristics, biochar can also be utilized as a low-cost adsorbent for aqueous contaminants removal [9-11]. Several researches have been conducted to evaluate the adsorption ability of biochar for P. However, the raw biochar without any treatment usually showed low capacity for P adsorption [12-14]. For instance, Zeng et al. [15] studied the sorption of phosphate from aqueous solution by four phytoremediation plants and the results suggested that these biochar had little ability to adsorb phosphate from aqueous solutions (removal rate < 40% at initial P concentrations of 30 mg/L). Hale et al. [16] tested the sorption of phosphate-P by cacao shell biochar and found that there was no sorption of PO_4−P to either washed or rinsed biochar.

Several investigations suggested that the modified biochar produced from the pyrolysis of anaerobically digested biomass and synthesis of nanoparticles-biochar composites exhibited strong ability to bind phosphate in aqueous solutions. Yao et al. [17] reported that the removal of phosphate by biochar produced from anaerobically digested sugar beet tailings was enhanced by exchangeable cations (Ca^{2+} and Mg^{2+}) concentrated by anaerobic digestion and the large amount of colloidal and nano-sized periclase (MgO) on its enlarged surface (surface area = 449 m^2 g^{-1}). MgO-biochar nanocomposites were synthesized by several studies through the pyrolysis of magnesium (Mg) enriched tomato tissues [14, 18] and $MgCl_2$-pretreat biomass [19]. These MgO-biochar nanocomposites all

showed excellent adsorption ability to phosphates and MgO particles presented on the surface of biochar served as the main adsorption sites. Other nanoparticles-biochar composites were also produced for P adsorption, such as biochar/MgAl-LDH ultra-fine composites [20] and biochar/AlOOH nanocomposite [21].

Recent studies also used calcium to modify biochar and applied the Ca-impregnated biochars to remove various contaminants from aqueous solutions. Agrafioti et al. [22] investigated the production of Ca modified biochar for the removal of heavy metals from aqueous solutions and found that the modified biochar exhibited much better As(V) removal capacity compared to the non-impregnated biochars. Aguayo-Villarreal et al. [23] also found that the carbonization of pecan nut shells impregnated with $CaCl_2$ could improve the surface area of the biochar and increase the total pore volume of it. The Ca^{2+} existed on the surface was found to favor the adsorption of dye due to the electrostatic interaction between Ca^{2+} species and the dye molecules. In fact, calcium has been commonly used in calcium–phosphorus precipitation as a method of phosphorus removal due to its low cost and easy operation [3]. Therefore, the application of calcium to functionalize biochar may be a possible method to enhance its phosphate removal ability. In addition, after adsorption of P, the P-laden biochar could be applied as a slow-release fertilizer and amendment to enhance soil fertility and improve soil properties [14]. However, little information is available about the application of Ca-impregnated biochar for phosphate adsorption from aqueous solutions right now.

Ramie (*Boehmeria nivea* (L.) Gaud.) is widely planted in Asian countries [24], where its bark has been used for long as a textile fiber. In China, ramie is an important economic crop with a production of 500,000 t of fibers per year, which is 96–97% of the world production [25]. A plenty of stem will be

generated as the agriculture waste after bark stripping, which can be recycled as the raw biomass feedstock for biochar production. The overarching objective of this work was to evaluate the removal potential of ramie stem biochar for P and apply Ca to improve its adsorption ability. For the first time, the Ca-modified biochar was prepared using the stem of ramie. Furthermore, the characterizations of Ca-modified biochar were analyzed using elemental analyzer, scanning electron microscopy (SEM), BET specific surface analyzer, energy-dispersive X-ray analysis (EDS), Fourier transform infrared (FTIR) and zeta potential meter. The phosphate adsorption ability was tested using batch sorption experiments. A series of laboratory experiments and mathematical models were conducted to determine the mechanisms of P adsorption on Ca-modified biochar.

2. Methods

2.1. Materials

All chemical reagents used in this experiment were purchased at analytical reagent grade. All the solution was prepared using deionized (DI) water with a resistivity of 18.25 MΩ cm^{-1}. Ramie used in this study was originally collected from the Ramie Institute of Hunan Agricultural University in China. After the leaves and tops of ramie were removed, the remaining bark and stem were separated and washed with deionized (DI) water and dried at 80 °C in a drying oven for 24 h. The dried bark and stem were smashed to powder and sieved through 2 mm sieve, respectively, and then stored in airtight plastic containers for later use.

2.2. Preparation of adsorbents

In the present study, the two types of biomass (bark and stem of ramie) were firstly pretreated with calcium ion before pyrolysis to produce Ca-impregnated biochar. Specifically, 5.6 g calcium chloride

dehydrate ($CaCl_2 \cdot 2H_2O$) was dissolved in 200 mL deionized (DI) water, then 10.0 g biomass was immersed in the Ca solution and the mixture was left shaking for 24 h at room temperature. The mixture was then dried in an oven at 90 °C for 24 h and stored in airtight plastic containers for later pyrolysis. A tube furnace (SK-1200 °C, Tianjin Zhonghuan Test Electrical Furnace Co., LTD, China) was used to convert these samples into biochar. The dried samples were fed into a quartz glass tube (5 cm diameter, 20 cm long) designed to fit inside of the furnace. The chamber of tube furnace was sealed and replenished with N_2 (400 mL/min) to keep the inert atmosphere along with the pyrolysis process. The temperature was programmed to rise up to 500 °C at a rate of 7 °C/min and held at the peak temperature for 2 h before cooling to room temperature. The resulted biochars from Ca-pretreated ramie bark and ramie stem were referred as Ca-RBB and Ca-RSB, respectively. The pristine biochar produced from the ramie stem without Ca treatment was also produced under the same pyrolysis condition and referred as RSB.

2.3. Characterizations

The elemental analyses of RSB and Ca-RSB were carried out with an elemental analyzer (Vario EL III, Elementar, Germany). For FTIR analysis, about 1 mg of adsorbent was ground with 100 mg of KBr in an agate mortar. The FTIR spectra (Nicolet 5700 Spectrometer, USA) of the samples were recorded in the range of 4000–400 cm^{-1}. Specific surface area of adsorbents were measured in a Micromeritics TriStar II 3020 by nitrogen adsorption N_2 (77.3 K) and the total pore volume was measured based on the N_2 adsorption-desorption isotherms. The morphological structure of Ca-RSB was characterized by Quanta FEG 250 environmental scanning electron microscopy (SEM) equipped with an energy-dispersive X-ray analyzer (EDS) (AMETER, USA). The zero point charge of

Ca-RSB was determined using Electroacoustic Spectrometer (ZEN3600 Zetasizer, UK) varying solution pH from 2.0 to 10.0. The X-ray photoelectron spectroscopy (XPS) measurements were performed using an ESCALAB 250Xi X-ray photoelectron spectrometer (Thermo Fisher, USA).

2.4. Adsorption experiments

Adsorption kinetics were examined by mixing 0.1 g of adsorbent with 50 mL phosphate solution (100 mg/L) in 100 mL Erlenmeyer flask at room temperature (26 ± 0.5 °C). The solutions were shaken at regular intervals, and the adsorbed phosphate concentrations were determined by the ascorbic acid method (ESS Method 310.1) [26] using a spectrophotometer (PGENERAL T6, Beijing, China) after filtration of the solution.

Adsorption isotherm of phosphate onto Ca-RSB was determined by batch sorption experiment at room temperature (26 ± 0.5 °C) by mixing 0.1 g Ca-RSB with 50 mL phosphate solutions of different concentrations ranging from 10 to 400 mg/L in the 100 mL Erlenmeyer flask. The Erlenmeyer flask were shaken for 24 h, which was determined by kinetic experiments to reach adsorption equilibrium. The samples were then withdrawn and filtered to determine adsorbed phosphate concentrations by the same method. The postadsorption biochar samples were collected, rinsed with deionized water, and dried at 80 °C for further XPS measurements.

The effect of pH on the adsorption of phosphate was determined by adjusting the initial phosphate solution (100 mg L^{-1}) ranging from 2.0 to 10.0 using solutions of NaOH and HCl. The flasks were shaken for 24 h at room temperature. The samples were then filtered and the phosphate concentrations were analyzed spectrophotometrically by the same method after filtration.

2.5. Statistical Analyses

147 The results shown in the figures represent the average of three independent replicate treatments.
148 The adsorption data obtained in this study are presented as means ± standard deviations (SD).

149 **3. Results and discussion**

150 3.1. Characterization of Ca-RSB

151 The physico-chemical characteristics of the RSB and Ca-RSB are shown in Table 1. The result of
152 elemental analysis showed that Ca-RSB exhibited lower carbon and nitrogen contents than RSB,
153 while much higher hydrogen content due to the introduction of Ca. As a result, the H/C ratio of
154 Ca-RSB significantly increased compared with RSB. The higher H/C ratio may indicate a lower
155 degree of carbonization [27, 28], which suggested that the impregnation of Ca may inhibit the
156 carbonization process and more functional groups may remain in the Ca-RSB [29]. In addition, a much
157 higher yield of Ca-RSB (50.8%) than RSB (28.0%) was also observed.

158 The characteristics of BET surface area are presented in Table 1. As can be seen, Ca-RSB (S_{BET} =
159 14.973 m^2/g, V_p = 0.057 $m^3\ g^{-1}$) exhibited much higher BET specific surface area (S_{BET}) and total
160 pore volume (V_p) than RSB (S_{BET} = 5.283 m^2/g, V_p = 0.013 $m^3\ g^{-1}$). Nitrogen adsorption–desorption
161 isotherm of Ca-RSB measured at 77.3 K is shown in Fig. 1a. According to the International Union of
162 Pure and Applied Chemistry (IUPAC) classification, the shape of isotherm was type II and IV [30, 31],
163 which suggested that Ca-RSB has meso- and macroporous structures [32]. This characteristic can also
164 be seen from the corresponding pore size distribution (Fig. 1b). The two materials had a similar pore
165 size distribution around 40−60 nm, however the pore volume of the Ca-RSB at this pore size range
166 was more than doubled due to Ca impregnation. In addition, new pore size distribution near 10-20
167 nm was occurred for Ca-RSB, which may be attributed to the increase of mesopore in Ca-RSB. The

observed hysteresis curves of Ca-RSB was type H4, indicating that narrow cracks and pores may exist in Ca-RSB [31, 32]. It's apparently that both the S_{BET} and V_p of the Ca-modified biochar were significantly increased, which may be beneficial to the adsorption capacity performance of Ca-RSB.

Analysis of surface morphology was conducted by scanning electron microscopy (SEM). Fig. S1 illustrates the SEM images of Ca-RSB. As can be seen, Ca-RSB exhibited irregular surfaces with pores of different shapes and sizes, and the calcium compounds were deposited on the biochar surfaces uniformly and smoothly. The result of the SEM-EDS analysis indicated the existence of calcium on the surface of Ca-RSB (Fig. 1c), which confirmed that the Ca was successfully impregnated into biochar.

The FTIR spectra of RSB and Ca-RSB are presented in Fig. 2. The intense band at 3000-3690 cm^{-1} was ascribed to the O−H stretching vibrations of hydrogen-bonded hydroxyl groups. The band at 1630 cm^{-1} was corresponding to C=C and C=O stretching vibrations [33]. The absorption peaks at 1403 cm^{-1} was assigned to –COO– symmetric stretching [34]. A minor band at 875 cm^{-1} was assigned to the γ–CH of furan [27]. The band at 555 cm^{-1} region were likely due to the M–O vibrations and M–O–H bending (M = Ca) [20, 35]. The FTIR spectra showed that Ca-RSB had much higher intensity of the bands of functional groups (−OH, −COO, C=C, C=O and M–O), which suggested that many original organic residues (such as cellulose, lignin and fatty acid) likely still remained in Ca-RSB and the introduction of Ca significantly increased the proportion of functional groups onto biochar, which may contribute to the higher adsorption ability of Ca-RSB.

3.2. Comparison experiments

The removal ability of phosphate by Ca-RSB and Ca-RBB were compared by mixing 0.1 g of adsorbent with 50 mL phosphate solution (100 mg/L) and measuring at regular intervals. As shown in Fig. 3a, the adsorption amount of Ca-RSB and Ca-RBB both increased along with the increase of time, and reached to the equilibrium around 840 min. However, Ca-RSB showed higher adsorption capacity than Ca-RBB through the whole adsorption process and a higher adsorption speed at the early stage. Considering the lower adsorption ability of Ca-RBB and the economic application of ramie bark (textile fiber), we choose Ca-RSB as the appropriate adsorbent for phosphate removal. The removal ability of pristine biochar (RSB) and Ca-modified biochar (Ca-RSB) were examined by varying the phosphate concentrations from 10 to 400 mg L^{-1}. As shown in Fig. 3b, the adsorption amount of Ca-RSB were more than two-folds than that of RSB at the varying phosphate concentrations, which suggested that the impregnation of Ca into biochar significantly increased the adsorption ability of phosphate. This might be mainly attributed to the increase of surface area, pore volume (Table 1 and Fig. 1) and functional groups (Fig. 2) of the Ca-RSB by introducing calcium particles onto biochar.

3.3. Effect of solution pH on phosphate adsorption

The initial solution pH significantly influenced the adsorption of the phosphate, which is a vital parameter in the optimization of adsorption process. The effect of pH on adsorption properties of phosphate by Ca-RSB were determined. As shown in Fig. 4, the adsorption amount of phosphate increased along with the increase of pH. The phosphate species varied with pH: mononuclear ($H_2PO_4^-$) at $0.12 < pH < 9.21$; binuclear (HPO_4^{2-}) at $5.21 < pH < 10.67$; trinuclear (PO_4^{3-}) at $10.67 < pH < 12$ [17]. Distribution of phosphate species as a function of solution pH was obtained using the

program Visual MINTEQ and the results (Fig. S2) demonstrated that the phosphate presented mainly in the form of H_3PO_4, $H_2PO_4^-$ and HPO_4^{2-} at pH range 2−10. At the initial low pH (pH = 2), the zeta potential was positive (Fig. 4) due to the protonation of various surface functional groups, that the negatively charged phosphate species $H_2PO_4^-$ could be electrostatically attracted by Ca-RSB. So that, electrostatic attraction served as the main force to adsorb phosphate at lower pH. As the increase of pH, the surface of Ca-RSB became negatively charged, which indicated that the function of electrostatic attraction decreased at higher pH and other banding forces took over.

3.4. Adsorption kinetics

Pseudo-first-order, pseudo-second-order and Elovich were applied to simulate the experimental kinetic data. The equations are generally expressed as follows [36, 37]:

$$\ln\left(q_e - q_t\right) = \ln q_e - k_1 t \quad (1)$$

$$\frac{t}{q_t} = \frac{1}{k_2 q_t^2} + \frac{t}{q_e} \quad (2)$$

$$q_t = \frac{1}{\beta}\ln(\alpha\beta t + 1) \quad (3)$$

where q_e (mg g^{-1}) and q_t (mg g^{-1}) represented the sorption amount of phosphate at equilibrium and at time t; k_1 (min^{-1}) and k_2 (g mg^{-1} min^{-1}) are the pseudo-first-order and pseudo-second-order reacted rate constant, respectively; α (mg/g) and β (mg/g) are the initial Elovich sorption and desorption rate constant, respectively. The results of adsorption kinetics studies are shown in Fig. 5a and the values of parameters are summarized in Table 2. The data showed a better fit to pseudo-second-order model (R^2 = 0.961) than pseudo-first-order model (R^2 = 0.893) and Elovich (R^2 = 0.959), which can be

further confirmed by the excellent accordance between the simulated results and experimental results, indicating that the chemisorption (such as chemical precipitation) of phosphate on Ca-RSB may be the rate-limiting mechanism [38].

Intra-particle diffusion model was further applied to determine the diffusion mechanisms and identify the possible rate controlling procedure. The intra-particle diffusion models equation is given as [36]:

$$q_t = k_{id} t^{1/2} + c_i \quad (4)$$

where q_t (mg g^{-1}) represented the sorption amount of phosphate at equilibrium and at time t, k_{id} is the intra-particle diffusion rate constant (mg/g·$min^{1/2}$), and c_i is the intercept related to the thickness of the boundary layer. As shown in Fig. 5b, the plots of q_t against $t^{1/2}$ are multi-linear including three linear portions, indicating that multiple steps were invol ved in the adsorption process. The values of c_i for all linear sections were not zero (Table 3), which suggested that intra-particle diffusion was one of the procedures involved in the adsorption process [36]. Phosphate was initially adsorbed by the exterior surface of the Ca-RSB during the adsorption process, so that the adsorption of phosphate onto Ca-RSB was firstly controlled by film diffusion. Then, the sorption process is controlled by intra-particle diffusion as phosphate further entered the pores of Ca-RSB and were subsequently adsorbed by the interior surfaces [39, 40].

To further decide the actual rate-controlling step involved in the whole phosphate sorption process, the Boyd kinetic model [41] were used to analyze the adsorption kinetic data, which is given by follows:

$$F = 1 - \frac{6}{\pi^2}\exp(-B_t) \quad (5)$$

Where F is the fraction of phosphate adsorbed at different time t. B_t is a mathematical function of F, which is expressed as:

$$F = \frac{q_t}{q_e} \quad (6)$$

Where q_e and q_t are the adsorption quantity at equilibrium and time t, respectively. The kinetic expression Eq. (6) can be represented as:

$$B_t = -0.4977 - \ln(1 - F) \quad (7)$$

Based on the analysis of the plot of this model, a reliable information about whether film diffusion or intraparticle diffusion is the actual rate-controlling step involved in the overall adsorption process will be provided. As shown in Fig. 5c, the plot of B_t versus t for the adsorption of phosphate onto Ca-RSB was a straight line and did not passing through the original point, which suggested that the film diffusion was the rate-controlling step in the initial adsorption process, and further other mechanisms (intra-particle diffusion) took over the rate-controlling role.

3.5. Adsorption isotherms

The adsorption equilibrium isotherms was studied using five commonly used isotherm equations including Langmuir, Freundlich, Langmuir−Freundlich, Redlich−Peterson and Temkin models to fit the experimental data (Fig. 6). These isotherms are expressed respectively by the following equations:

$$q_e = \frac{q_{max} K_l C_e}{1 + K_l C_e} \quad (8)$$

$$q_e = K_f C_e^{1/n} \quad (9)$$

$$q_e = \frac{q_{max} K_{lf} C_e^{n}}{1 + K_{lf} C_e^{n}} \quad (10)$$

$$q_e = \frac{K_r C_e}{1 + a C_e^{n}} \quad (11)$$

$$q_e = \frac{RT}{b} \ln(A C_e) \quad (12)$$

Where q_e is the amount of the phosphate adsorbed (mg/g), C_e is the equilibrium concentration of solution (mg/L), q_{max} is the maximum adsorption capacity (mg/g), and K_l is the Langmuir constant related to the affinity. K_f and $1/n$ are the Freundlich constants, which indicate the adsorption capacity and intensity, respectively. K_{lf} and n are the Langmuir-Freundlich affinity parameter and constant, respectively. K_r and a are the Redlich-Peterson isotherm constants. A ($L \cdot mg^{-1}$) and b ($J \cdot g \cdot mg^{-1}$) are the Temkin isotherm constants. The model parameters and the corresponding correlation coefficient (R^2) for the five different models are summarized in Table 4. It can be seen that the isotherm data of phosphate adsorption by Ca-RSB was fitted better by Langmuir model (R^2 = 0.983) than other models, indicating that the adsorption of phosphate onto the Ca-RSB surface was probably a monolayer adsorption onto a homogeneous surface [14].

Based on the Langmuir model, the maximum phosphate adsorption capacity was 105.406 mg/g, which confirmed the high adsorption capability of Ca-RSB. The comparisons of maximum adsorption capacities of Ca-RSB of this study with other adsorbents reported previously for the adsorption of phosphate are listed in Table 5. As shown in the table, the phosphate adsorption

capacity of Ca-RSB is comparable to that of Mg-biochar nanocomposite prepared by pyrolyzing Mg-enriched tomato leaves [14] and much higher than that of other adsorbents. Such comparison also suggests that Ca-RSB may be an effective and low-cost adsorbent for phosphate removal from contaminated water.

3.6. Adsorption mechanisms

The excellent adsorption performance of Ca-RSB might be attributed to the improvement of various physical/chemical properties including much higher content of total pore volume, BET surface area and functional groups, as well as the introduction of Ca on the biochar surface. The calcium ions may attach onto the surface or get into the interior of biomass after it is dipped into the calcium salts solution. After pyrolysis, the calcium ions will transform into CaO nano-particles, and the biomass impregnated with calcium ions will become CaO-biochar nanocomposite. The results of FTIR spectra (Fig. 2) and XPS (Fig. 8) revealed that CaO nano-particles were formed on the surface of biochar after pyrolysis, which may contribute to the higher total pore volume and BET surface area. The nanosized CaO nano-particles grown on biochar surfaces dramatically increased the reactive area and sites to attract phosphate from water. In addition, $CaCl_2$ could serve as flame retardants, which may enhance biochar yields as well as promoting its surface oxygen-containing functional groups. Three mechanisms mainly involved in the adsorption process (Fig. 7).

At lower pH, the negatively charged phosphate species $H_2PO_4^-$ could be electrostatically attracted by positive Ca-RSB surface. At the pH range in our study, phosphate in the solution mainly exists in the species of HPO_4^{2-} and HPO_4^-, which would precipitate the released Ca to form the $CaHPO_4$ and $Ca(H_2PO_4)_2$ crystals. However, $CaHPO_4$ and $Ca(H_2PO_4)_2$ were easily dissolved in acid solution,

306 which lead to the lower removal performance for phosphate. Therefore, electrostatic attraction served
307 as the main force to adsorb phosphate at lower pH. With the increase of pH, these crystals became
308 less soluble and precipitation exerted more effect on P sorption.

309 The chemical precipitation of P on the biochar was further confirmed by XPS analysis (Fig. 8).
310 The Ca 2p spectrum (Fig. 8a) demonstrated that three compounds were presented on the P laden
311 biochar surface. The binding energy at 347.5 eV corresponds to $CaHPO_4$, while that at 347.8 eV
312 corresponds to $Ca(H_2PO_4)_2$ [42, 43]. The XPS spectrum of P 2p on the surface of the P-laden biochar
313 (Fig. 8b) also revealed the formation of $CaHPO_4$ and $Ca(H_2PO_4)_2$ crystals on biochar surface. The
314 binding energy at 133.5 eV corresponds to $CaHPO_4$, while that at 134.0 eV corresponds to
315 $Ca(H_2PO_4)_2$ [42, 43]. This significant change after P sorption suggested that precipitation played an
316 important role in P removal by Ca-RSB. In addition, it can be obviously observed that CaO (Ca 2p
317 spectrum at 351.2 eV) [44] and $H_2PO_4^-$ (P 2p spectrum at 134.7 eV) [45] were still existed on biochar
318 surface, which can be attributed to the surface deposition mechanisms of the interaction between P
319 and CaO particles. Furthermore, the two precipitates (i.e., $CaHPO_4$ and $Ca(H_2PO_4)_2$ particles) may
320 also adsorb additional P anion by hydrogen bonding [14, 46]. These results indicated that, surface
321 deposition could also play an important role in promoting P adsorption onto Ca-RSB.

322 **4. Conclusions**

323 The Ca-impregnated biochar was successfully synthesized through pyrolysis of $CaCl_2$ pre-treated
324 biomass (ramie, *Boehmeria nivea* (L.) Gaud.). Ramie stem and bark can both be used as biomass
325 feedstock, while ramie stem is more suitable for biochar production than ramie bark considering its
326 higher adsorption ability and economic feasibility. Ca-impregnated biochar had much higher H/C

ratio, total pore volume, BET surface area, functional groups and yield rate than the pristine biochar. The impregnation of Ca significantly increased the efficiency for phosphate removal from aqueous solutions with the high adsorption ability > 100 mg/g. The results of this study suggested that Ca-impregnated biochar can be used as a potential high-efficiency and low-cost adsorbent for mitigating eutrophication using adsorption technology.

Acknowledgments

The authors would like to thank financial support from the National Natural Science Foundation of China (Grant No. 41271332 and 51521006), and the Hunan Provincial Innovation Foundation For Postgraduate (Grant No. CX2015B090 and CX2015B092).

References

1. D. L. Correll, *J. Environ. Qual.*, 1998, **27**, 261-266.
2. V. H. Smith, *Environ. Sci. Pollut. Res.*, 2003, **10**, 126-139.
3. L. E. de-Bashan and Y. Bashan, *Water Res.*, 2004, **38**, 4222-4246.
4. G. K. Morse, S. W. Brett, J. A. Guy and J. N. Lester, *Sci. Total Environ.*, 1998, **212**, 69-81.
5. J. Lehmann and S. Joseph, *Biochar for environmental management: science and technology*, Routledge, 2012.
6. S. Meyer, B. Glaser and P. Quicker, *Environ. Sci. Technol.*, 2011, **45**, 9473-9483.
7. J. Lehmann, *Nature*, 2007, **447**, 143-144.
8. S. P. Sohi, *Science*, 2012, **338**, 1034-1035.
9. X. Tan, Y. Liu, G. Zeng, X. Wang, X. Hu, Y. Gu and Z. Yang, *Chemosphere*, 2015, **125**, 70-85.
10. C. Gan, Y. Liu, X. Tan, S. Wang, G. Zeng, B. Zheng, T. Li, Z. Jiang and W. Liu, *RSC Adv.*, 2015, **5**, 35107-35115.
11. M.M. Zhang, Y.G. Liu, T.T. Li, W.H. Xu, B.H. Zheng, X.F. Tan, H. Wang, Y.M. Guo, F.Y. Guo and S.F. Wang, *RSC Adv.*, 2015, **5**, 46955-46964.
12. Y. Yao, B. Gao, M. Zhang, M. Inyang and A. R. Zimmerman, *Chemosphere*, 2012, **89**, 1467-1471.
13. M. Morales, N. Comerford, I. Guerrini, N. Falcão and J. Reeves, *Soil Use Manage.*, 2013, **29**, 306-314.
14. Y. Yao, B. Gao, J. Chen and L. Yang, *Environ. Sci. Technol.*, 2013, **47**, 8700-8708.

15. Z. Zeng, T.Q. Li, F.L. Zhao, Z.L. He, H.P. Zhao, X.E. Yang, H.L. Wang, J. Zhao and M. T. Rafiq, *J. Zhejiang Univ. Sci. B*, 2013, **14**, 1152-1161.

16. S. Hale, V. Alling, V. Martinsen, J. Mulder, G. Breedveld and G. Cornelissen, *Chemosphere*, 2013, **91**, 1612-1619.

17. Y. Yao, B. Gao, M. Inyang, A. R. Zimmerman, X. Cao, P. Pullammanappallil and L. Yang, *J. Hazard. Mater.*, 2011, **190**, 501-507.

18. Y. Yao, B. Gao, J. Chen, M. Zhang, M. Inyang, Y. Li, A. Alva and L. Yang, *Bioresour. Technol.*, 2013, **138**, 8-13.

19. M. Zhang, B. Gao, Y. Yao, Y. Xue and M. Inyang, *Chem. Eng. J.*, 2012, **210**, 26-32.

20. M. Zhang, B. Gao, Y. Yao and M. Inyang, *Chemosphere*, 2013, **92**, 1042-1047.

21. M. Zhang and B. Gao, *Chem. Eng. J.*, 2013, **226**, 286-292.

22. E. Agrafioti, D. Kalderis and E. Diamadopoulos, *J. Environ. Manage.*, 2014, **146**, 444-450.

23. I. Aguayo-Villarreal, V. Hernández-Montoya, N. Rangel-Vázquez and M. Montes-Morán, *J. Mol. Liq.*, 2014, **196**, 326-333.

24. Z. Sun, Y. Liu, Y. Huang, G. Zeng, Y. Wang, X. Hu and L. Zhou, *Ecol. Eng.*, 2014, **71**, 108-112.

25. E. Kipriotis, X. Heping, T. Vafeiadakis, M. Kiprioti and E. Alexopoulou, *Ind. Crop. Prod.*, 2015, **68**, 126-130.

26. USEPA, *Environmental Sciences Section Inorganic chemistry unit, Wisconsin State Lab of Hygiene*, 1992.

27. X. Chen, G. Chen, L. Chen, Y. Chen, J. Lehmann, M. B. McBride and A. G. Hay, *Bioresour. Technol.*, 2011, **102**, 8877-8884.

28. T. Kuhlbusch, *Environ. Sci. Technol.*, 1995, **29**, 2695-2702.

29. Z. Chen, B. Chen and C. T. Chiou, *Environ. Sci. Technol.*, 2012, **46**, 11104-11111.

30. F. B. D. Saiah, B.-L. Su and N. Bettahar, *J. Hazard. Mater.*, 2009, **165**, 206-217.

31. X. Zhao, W. Ouyang, F. Hao, C. Lin, F. Wang, S. Han and X. Geng, *Bioresour. Technol.*, 2013, **147**, 338-344.

32. X.R. Jing, Y.Y. Wang, W.J. Liu, Y.K. Wang and H. Jiang, *Chem. Eng. J.*, 2014, **248**, 168-174.

33. Y.J. Zhang, Z.J. Xing, Z.K. Duan, M. Li and Y. Wang, *Appl. Surf. Sci.*, 2014, **315**, 279-286.

34. J. Tang, K. W. Kemp, S. Hoogland, K. S. Jeong, H. Liu, L. Levina, M. Furukawa, X. Wang, R. Debnath and D. Cha, *Nat. mater.*, 2011, **10**, 765-771.

35. K.H. Goh, T.T. Lim, A. Banas and Z. Dong, *J. Hazard. Mater.*, 2010, **179**, 818-827.

36. X.J. Hu, J.S. Wang, Y.G. Liu, X. Li, G.M. Zeng, Z.L. Bao, X.X. Zeng, A.W. Chen and F. Long, *J. Hazard. Mater.*, 2011, **185**, 306-314.

37. Y. Xue, B. Gao, Y. Yao, M. Inyang, M. Zhang, A. R. Zimmerman and K. S. Ro, *Chem. Eng. J.*, 2012, **200**, 673-680.

38. H. Lu, W. Zhang, Y. Yang, X. Huang, S. Wang and R. Qiu, *Water Res.*, 2012, **46**, 854-862.

39. L. Ai, C. Zhang and L. Meng, *J. Chem. Eng. Data*, 2011, **56**, 4217-4225.

40. Z. Wu, H. Zhong, X. Yuan, H. Wang, L. Wang, X. Chen, G. Zeng and Y. Wu, *Water Res.*, 2014, **67**, 330-344.

41. G. Boyd, A. Adamson and L. Myers Jr, *JACS*, 1947, **69**, 2836-2848.

42. T. Hanawa and M. Ota, *Biomaterials*, 1991, **12**, 767-774.

43. Y. Barbaux, M. Dekiouk, D. Le Maguer, L. Gengembre, D. Huchette and J. Grimblot, *Appl. Catal. A: Gen.*, 1992, **90**, 51-60.

44. W. Zhang, K. Du, C. Yan and F. Wang, *Appl. Surf. Sci.*, 2008, **254**, 5216-5223.

45. Q. Wang, H. Yu, L. Zhong, J. Liu, J. Sun and J. Shen, *Chem. Mater.*, 2006, **18**, 1988-1994.

46. C. C. Chusuei, D. Goodman, M. Van Stipdonk, D. Justes, K. Loh and E. Schweikert, *Langmuir*, 1999, **15**, 7355-7360.

47. S. Vasudevan and J. Lakshmi, *RSC Adv.*, 2012, **2**, 5234-5242.

48. X. Liu and L. Zhang, *Powder Technol.*, 2015, **277**, 112-119.

49. L. Chen, X. Zhao, B. Pan, W. Zhang, M. Hua, L. Lv and W. Zhang, *J. Hazard. Mater.*, 2015, **284**, 35-42.

50. L. Zhang, Q. Zhou, J. Liu, N. Chang, L. Wan and J. Chen, *Chem. Eng. J.*, 2012, **185–186**, 160-167.

51. F. Peng, P.W. He, Y. Luo, X. Lu, Y. Liang and J. Fu, *CLEAN – Soil, Air, Water*, 2012, **40**, 493-498.

52. S.Y. Yoon, C.G. Lee, J.A. Park, J.H. Kim, S.B. Kim, S.H. Lee and J.W. Choi, *Chem. Eng. J.*, 2014, **236**, 341-347.

418 Table 1. Physico-chemical characteristics of RSB and Ca-RSB.

Biochars	Elemental composition (%, mass based)				S_{BET} [a]	V_{RSB}	W_p [c]	Yield (%)
	C	H	N	H/C				
RSB	63.34	1.870	0.617	0.354	5.283	0.013	9.943	28.0
Ca-RSB	18.49	6.301	0.210	4.089	14.973	0.057	13.584	50.8

419 [a] BET specific surface area (m^2/g)

420 [b] Total pore volume ($P/P_o = 0.9969$, cm^3/g)

421 [c] Adsorption average pore width (4V/A by BET, nm)

422

423 Table 2. The model parameters and the corresponding correlation coefficient of kinetics models.

	parameter 1	parameter 2	R^2
Pseudo-first-order	$q_e = 35.223 \pm 1.167$	$k_1 = 0.028 \pm 0.004$	0.893
Pseudo-second-order	$q_e = 37.211 \pm 0.827$	$k_2 = 1.160\times10^{-3} \pm 1.520\times10^{-4}$	0.961
Elovich	$\alpha = 8.206 \pm 2.426$	$\beta = 0.191 \pm 0.012$	0.959

424

425 Table 3. Intra-particle diffusion parameters for the adsorption of phosphate by calcined
426 biochar/MgAl-LDH.

	k_{id} (mg/g·$h^{1/2}$)	c_i	R_i^2
Section1	2.288 ± 0.070	6.425 ± 0.438	0.994
Section2	0.492 ± 0.059	25.870 ± 0.907	0.972
Section3	0.120 ± 0.012	32.993 ± 0.343	0.951

427

428 Table 4. The model parameters and the corresponding correlation coefficient of isotherm models.

	parameter 1	parameter 2	parameter 3	R^2
Langmuir	q_{max} = 105.406 ± 5.446	K_l = 0.039 ± 0.007		0.983
Freundlich	1/n = 0.416 ± 0.061	K_f = 11.200 ± 3.273		0.936
Langmuir−Freundlich	q_{max} = 102.462 ± 11.073	K_{lf} = 0.036 ± 0.017	n= 1.058 ± 0.228	0.979
Redlich−Peterson	a = 0.055 ± 0.056	K_r = 4.466 ± 1.355	n= 0.950 ± 0.140	0.979
Temkin	b = 122.126 ± 7.630	A = 0.534 ± 0.096		0.977

429

430 Table 5. Maximum adsorption capacities for phosphate onto various adsorbents.

Adsorbent	Temperature (K)	q_{max} (mg/g)	References
Ca impregnated biochar	299	105.41	In this study
Mg-biochar nanocomposite	295	103.80	[14]
Graphene	303	89.37	[47]
Zirconic chitosan beads	288	61.70	[48]
Hydrous zirconium oxide-based nanocomposite	303	27.80	[49]
Lanthanum hydroxide-doped activated carbon fiber	–	15.30	[50]
Pine sawdust char	298	15.11	[51]
Magnetic iron oxide nanoparticles	303	5.03	[52]

431

432

433 **Figure captions**

434 **Fig. 1.** Properties of biochar: (a) nitrogen adsorption-desorption isotherms of Ca-RSB; (b) pore size
435 distribution of RSB and Ca-RSB; (c) SEM-EDS analysis of Ca-RSB.

436 **Fig. 2.** FTIR spectra of RSB and Ca-RSB.

437 **Fig. 3.** Comparison experiments: (a) removal ability of phosphate by Ca-RSB and Ca-RBB; (b) removal
438 ability of phosphate by Ca-RSB and RSB.

439 **Fig. 4.** Zeta potentials of Ca-RSB at different pH and effect of pH on the adsorption of phosphate by
440 Ca-RSB.

441 **Fig. 5.** (a) The kinetics for phosphate adsorbed by Ca-RSB; (b) Intraparticle diffusion plots of
442 adsorption capacity q_t versus the square root of time $t^{0.5}$ for the adsorption of phosphate onto Ca-RSB;
443 (c) Plots of Boyd parameter B_t versus time t for the adsorption of phosphate onto Ca-RSB.

444 **Fig. 6**. The equilibrium isotherms for phosphate adsorbed by Ca-RSB.

445 **Fig. 7.** Mechanisms of phosphate adsorption onto Ca-RSB.

446 **Fig. 8**. XPS spectra of (a) Ca 2p and (b) P 2p of Ca-RSB after P adsorption.

447

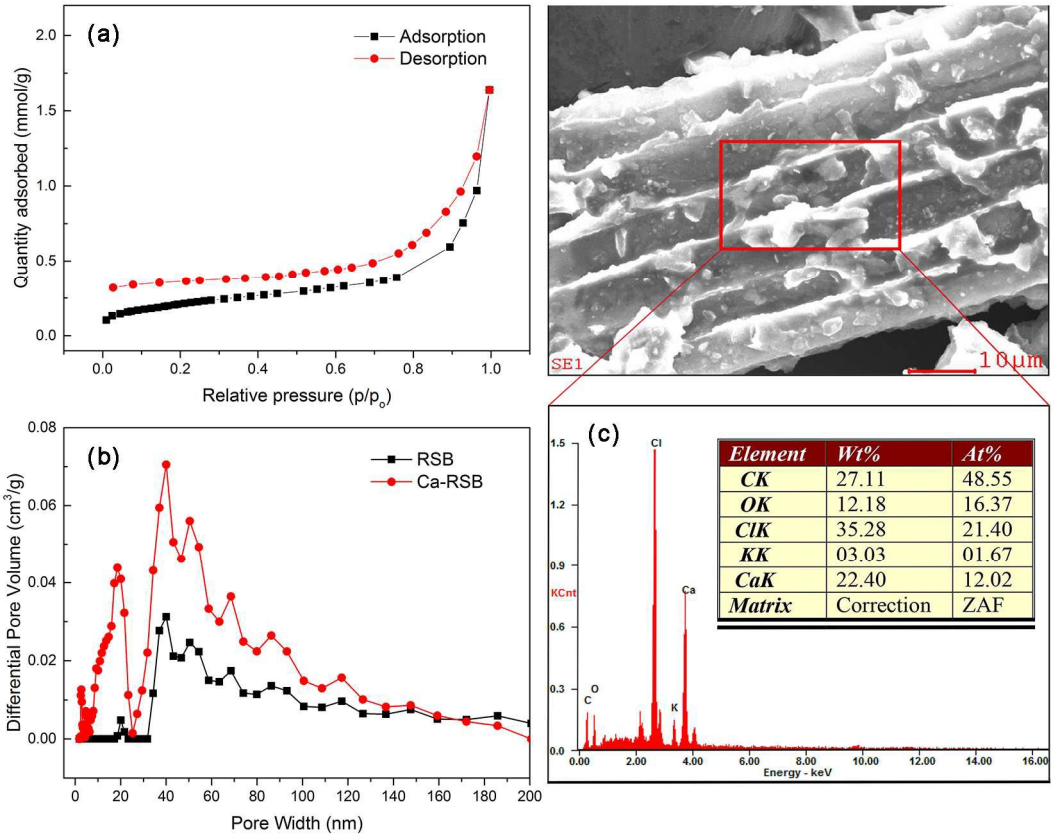

448

449 **Fig. 1.** Properties of biochar: (a) nitrogen adsorption-desorption isotherms of Ca-RSB; (b) pore size

450 distribution of RSB and Ca-RSB; (c) SEM-EDS analysis of Ca-RSB.

451

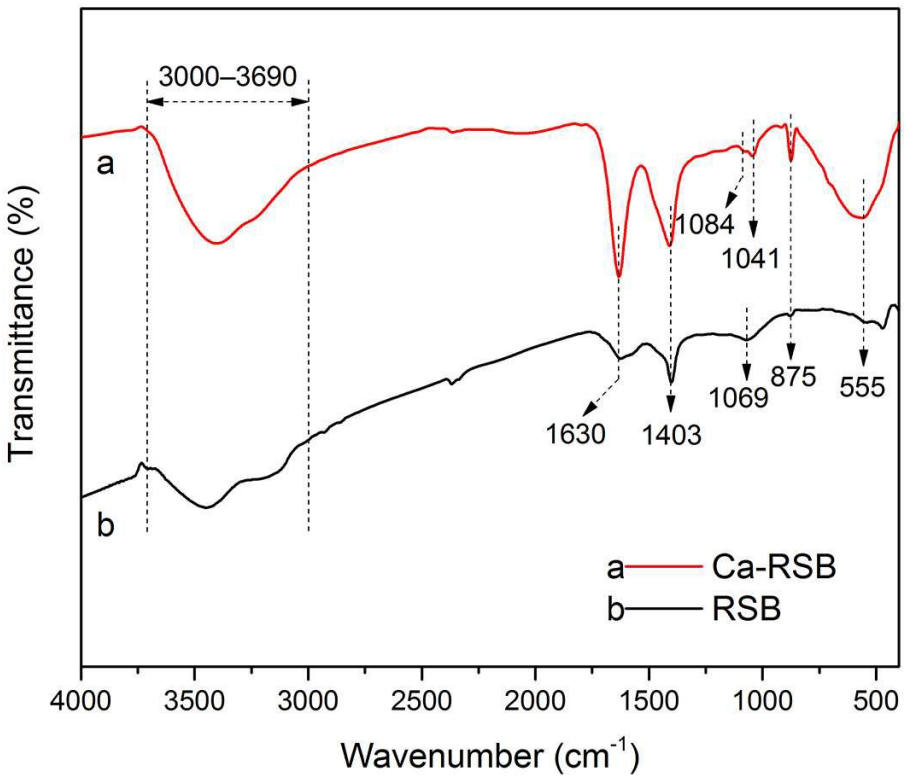

452

453 **Fig. 2.** FTIR spectra of RSB and Ca-RSB.

454

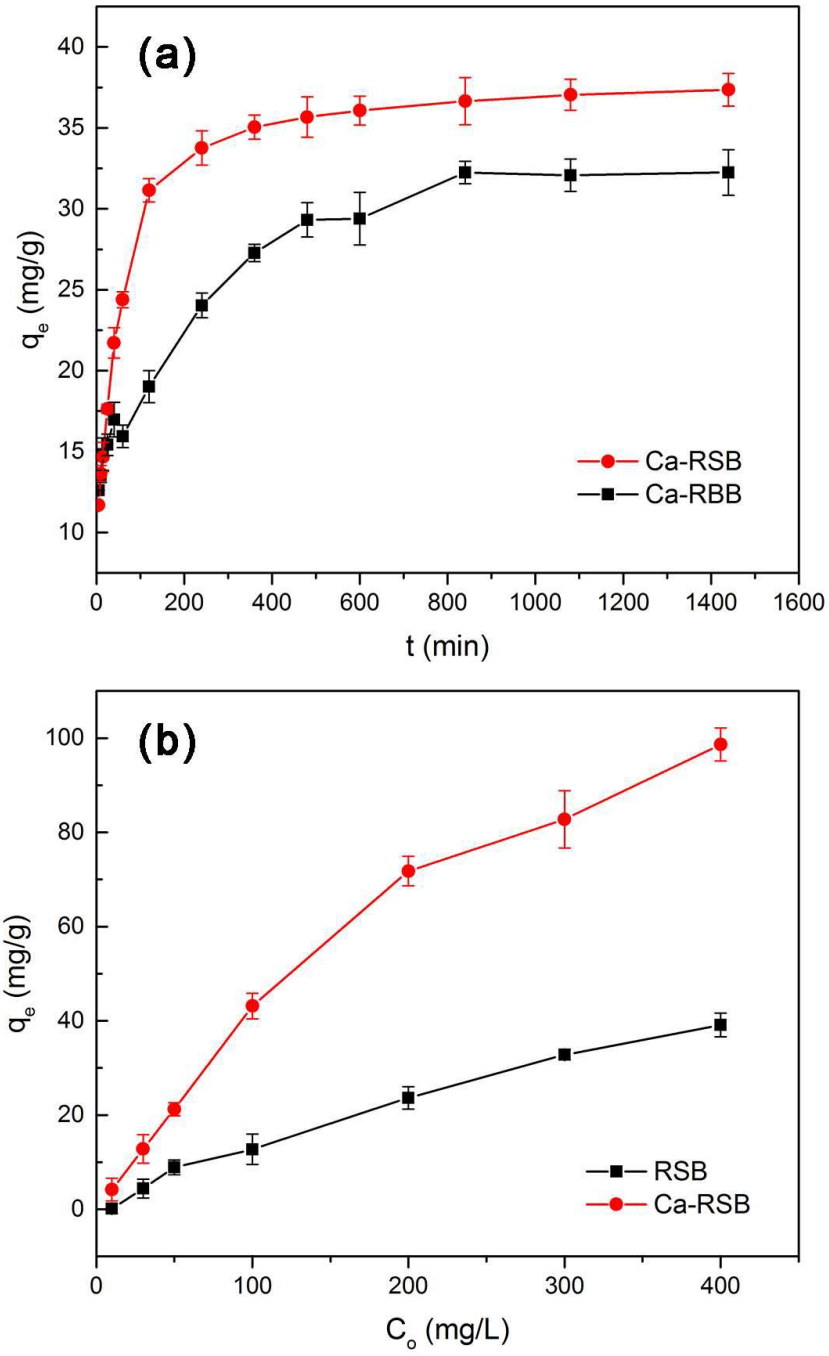

455

456 **Fig. 3.** Comparison experiments: (a) removal ability of phosphate by Ca-RSB and Ca-RBB; (b) removal

457 ability of phosphate by Ca-RSB and RSB.

458

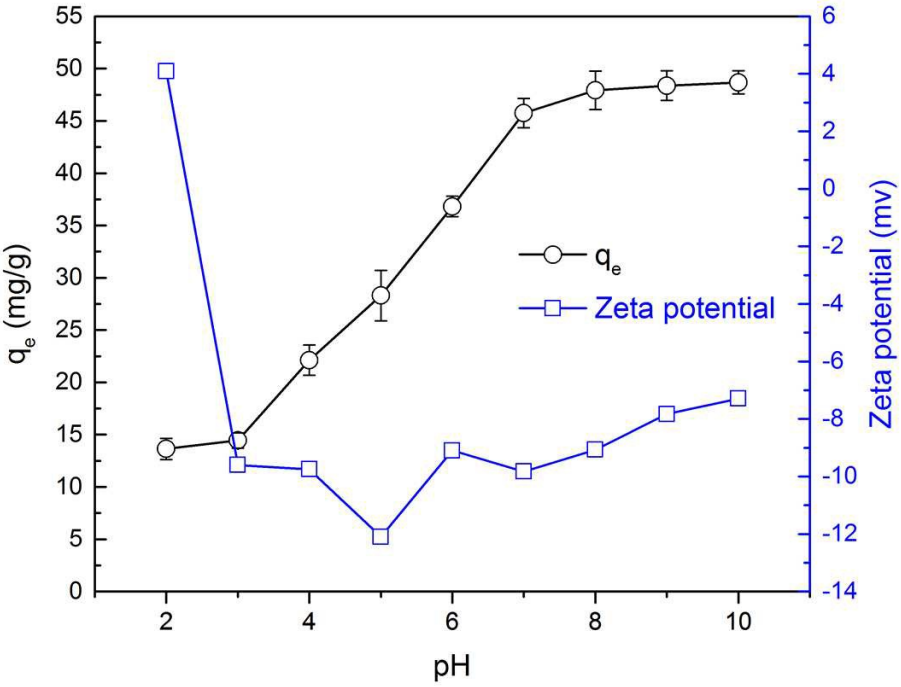

459

460 **Fig. 4.** Zeta potentials of Ca-RSB at different pH and effect of pH on the adsorption of phosphate by

461 Ca-RSB.

462

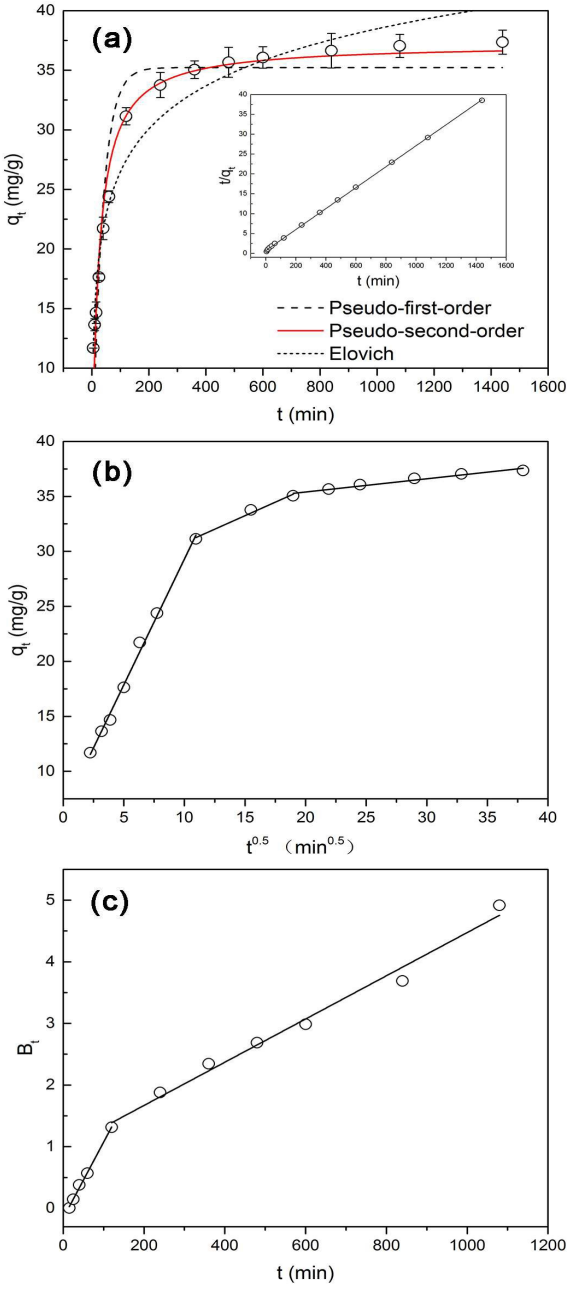

463

464 **Fig. 5.** (a) The kinetics for phosphate adsorbed by Ca-RSB; (b) Intraparticle diffusion plots of

465 adsorption capacity q_t versus the square root of time $t^{0.5}$ for the adsorption of phosphate onto Ca-RSB;

466 (c) Plots of Boyd parameter B_t versus time t for the adsorption of phosphate onto Ca-RSB.

467

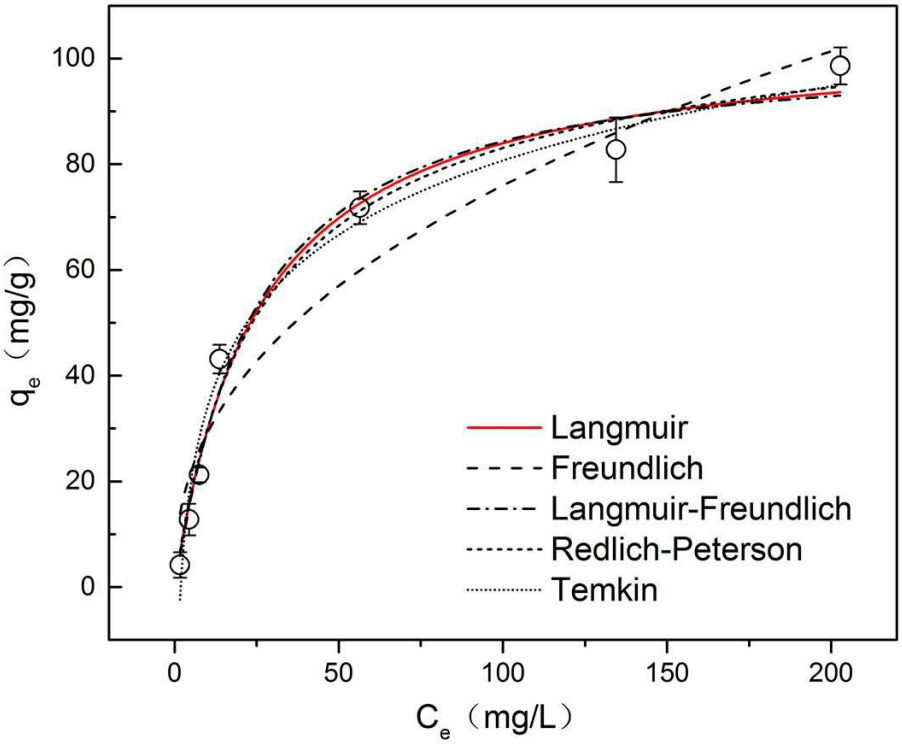

468

469 **Fig. 6.** The equilibrium isotherms for phosphate adsorbed by Ca-RSB.

470

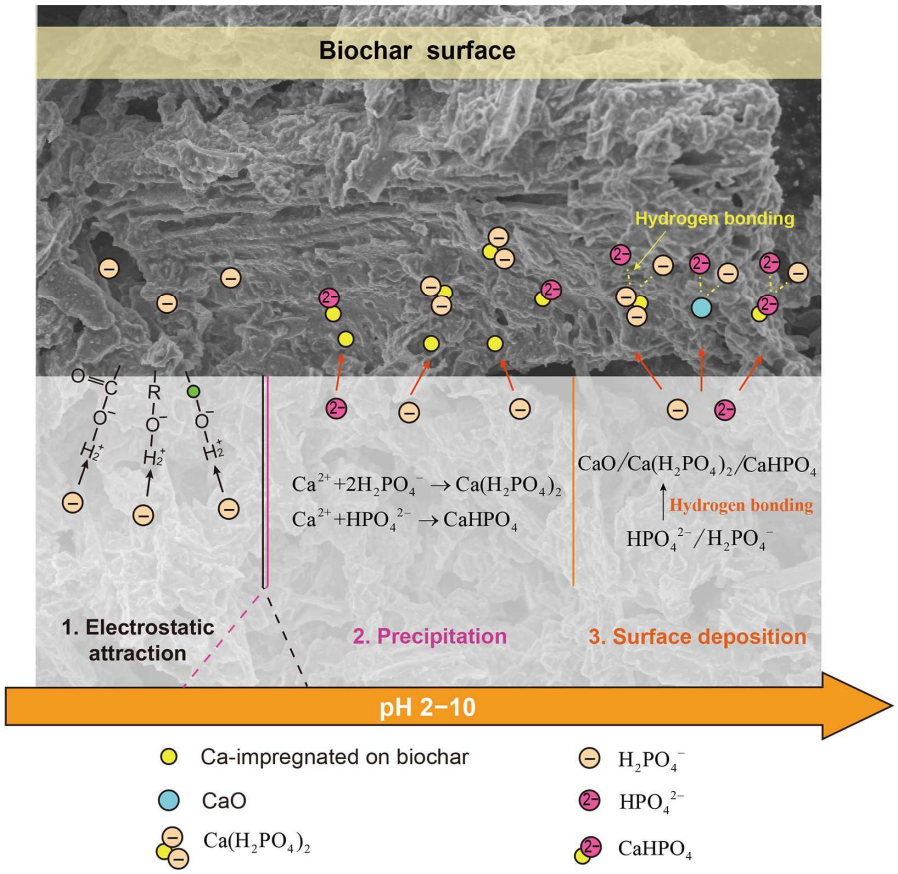

471

472 **Fig. 7.** Mechanisms of phosphate adsorption onto Ca-RSB.

473

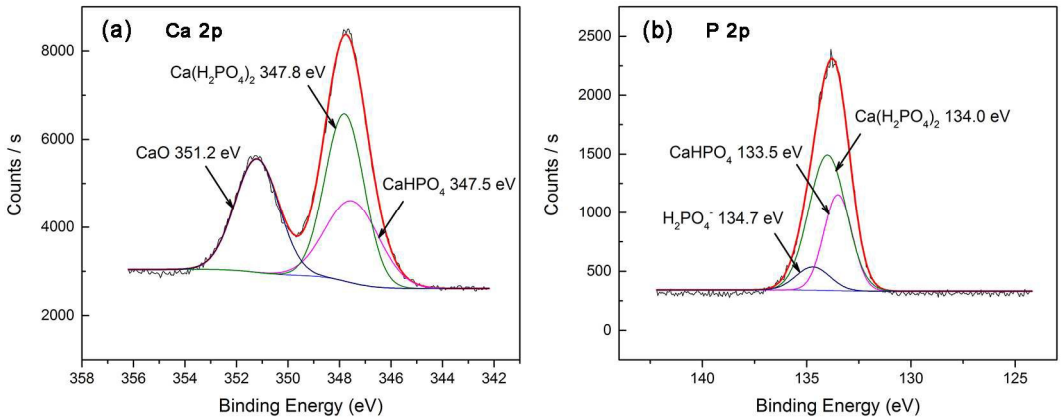

474

475 **Fig. 8**. XPS spectra of (a) Ca 2p and (b) P 2p of Ca-RSB after P adsorption.